UNDERSTANDING DEFECT GUIDANCE IN KAGOME-CLAD STRUCTURES

A Thesis

by

HECTOR PEREZ

Submitted to the Office of Graduate and Professional Studies of
Texas A&M University
in partial fulfillment of the requirements for the degree of

MASTER OF SCIENCE

Chair of Committee,	Aleksei Zheltikov
Committee Members,	Philip Hemmer
	Olga Kocharovskaya
	Alexei Sokolov
Head of Department,	George R Welch

August 2016

Major Subject: Physics

ABSTRACT

In this work we study structural features of interest in the kagome lattice in order to provide a better understanding of out-of-plane guidance of light within a defect in a kagome lattice cladding. With the aid of electromagnetic simulation we build and compare dispersion maps of select electromagnetic modes found within the hexagonal air-holes of the lattice and modes found in defects introduced into the lattice. Then, with the self-similarity of the lattice in mind, we arrive at a geometric explanation for the appearance of defect guided modes within the continuum of cladding states. Additionally, we study subsets of the kagome lattice related to band-gap structures to see their influence on dispersion and show that regions of guidance are influenced by band-gaps which appear for a subset of the kagome lattice. With these insights we provide design considerations to further decrease loss and widen regions of guidance in kagome-clad fibers.

DEDICATION

I dedicate this work to everyone that has provided their support or guidance on my journey through life.

ACKNOWLEDGEMENTS

This research was supported in part by the Welch Foundation (Grant No. A-1801) and the Russian Foundation for Basic Research (project nos. 13-02-01465 and 14-29-07182). Research into waveguides for the mid-infrared range was supported by the Russian Science Foundation (project no. 14-12-00772).

TABLE OF CONTENTS

Page

LIST OF FIGURES

FIGURE Page

1. INTRODUCTION*

In recent times the kagome fiber has emerged as part of a class of optical fiber which supports guided modes within it's core, where these guided modes exist in a continuum of cladding states. These types of fibers are inherently lossier than those guiding via photonic band-gap (PBG), and while increasing the number of cladding rings in a PBG fiber has a pronounced effect on loss, there is some debate regarding the role played by the cladding rings in a kagome clad fiber [1–3]. The advantage, however, is that they display a much broader range of guidance [4–6]. For example, hollow fibers with a kagome cladding have been shown to enable efficient multioctave supercontinuum generation [7] and pulse compression to sub cycle pulse widths and gigawatt peak powers [8]. Guidance in this case is usually attributed to an inhibited coupling between the core and cladding modes resulting from either a large phase mismatch or low spatial overlap between the two modes [4], as in Fig. 1.1 for example. The high loss regions occur around resonances of the glass immediately surrounding the core [2,9] where lattice modes approach their cutoff [10], and additionally no guided modes are found at the lower frequency edge [7]. While this description has had success in that it provides an avenue to lower loss through further inhibiting coupling, as can be seen in hypocycloid core designs [3, 11–13], it fails to explain why the defect modes appear within the continuum of cladding states in the first place or why they are found at the points in the continuum that they are. There is mention of the defect modes' relation to Von Neumann-Wigner bound states [7]–states built up by diffractive interference from a local potential [14]–but

*Sections of text reprinted with permission from "Modal analysis of kagome-lattice structures" by H Perez, S Blakley, A M Zheltikov, 2015. Laser Phys. Lett., 12, 055102–055108, Copyright 2015 by IOP Publishing.

no further discussion of the characteristics of the potential which enables them to exist in this case. The guidance characteristics of microstructured fibers have been shown to have a sensitive dependence on the cross-sectional geometry [15] which can be illustrated by the following example pictured in Fig. 1.2: beginning with the same triangular tube lattice preform, pressurizing either only the inside of the tubes or instead all of the hollow regions during the draw we can produce either a PBG fiber [15–21] or a kagome [4, 11, 22, 23] fiber, respectively, the two of which guide light in fundamentally different ways [1, 4, 24]. In this work we study the influence of structural features of the kagome lattice on guidance in a defect with the help of a freely available software package which computes fully-vectorial eigenmodes of Maxwell's equations with periodic boundary conditions by preconditioned conjugate-gradient minimization of the block Rayleigh quotient in a plane wave basis [25]. One set of features we explore are those related to PBGs, inspired by an account in the literature stating that an arrangement of rods placed at the node sites in the kagome lattice gives rise to band-gaps [26], as well as the concentric hexagon model used in [1, 2] which is shown to have a similar loss profile compared to the full structure, even though the guidance characteristics of the simplified model bear more similarity to the band-gap structure it approximates. Despite the kagome cladding lacking PBGs, we shall provide evidence that band-gaps influence guidance characteristics and density of states (DOS). The other structural feature we explore is inherent to the kagome lattice, namely, the self-similarity at different length scales. Taking a kagome lattice and scaling it up to a new lattice pitch $\Lambda' = m\Lambda$ where m is an odd number, we can take this blown up structure and fit it over our original structure as exemplified by Fig. 1.3. This leads us to a geometric explanation for the appearance of guided modes and we see that this also affects the density of cladding states and regions of guidance.

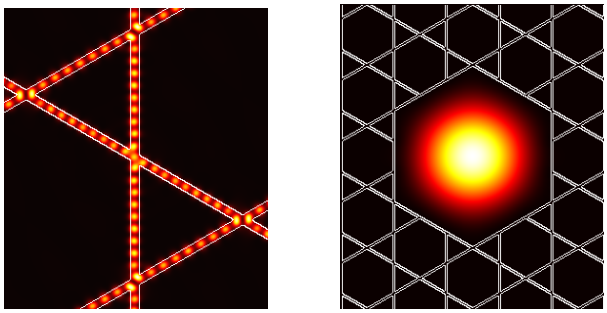

(a) (b)

Figure 1.1: (a) Fast oscillations of the cladding mode vs (b) the fundamental defect mode.

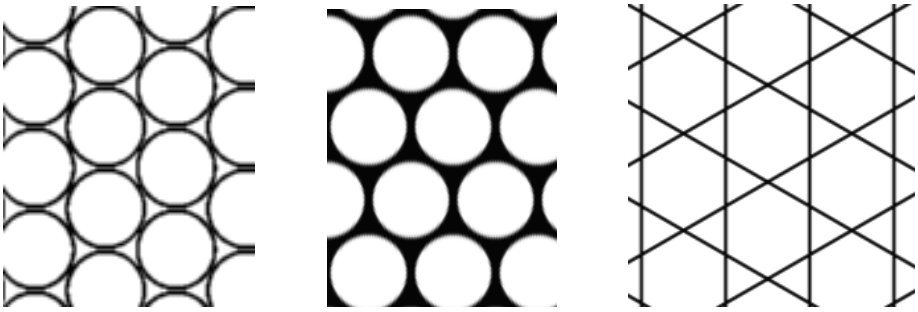

(a) (b) (c)

Figure 1.2: (a) An arrangement of tubes stacked into a triangular lattice can be drawn to either (b) a PBG geometry or (c) a kagome lattice, the two of which can be used to guide light in fundamentally different ways.

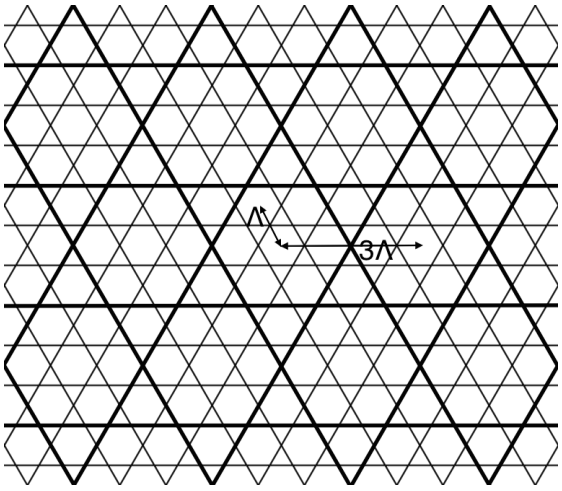

Figure 1.3: Kagome lattice with a larger scale kagome lattice overlaid and bolded for clarity

2. SIMULATION RESULTS

Throughout our simulations the glass index was kept at a constant n = 1.4585 corresponding to the index of silica glass between the ultraviolet and mid-IR [27]. In order to test the influence of the cladding on defect guided modes we simulated modes for four different core sizes in two orientations as compared to the surrounding lattice. These are shown below in Fig. 2.1. Modes were identified based on their transverse power profile and we considered mainly the fundamental mode and the second and third order circularly symmetric modes of the defect as well as lattice modes of the same symmetry which appeared in the hexagonal air holes. The computed modes have normalized frequency $\alpha = \Lambda/\lambda$, where we have taken Λ to be the lattice pitch and λ is the free space wavelength.

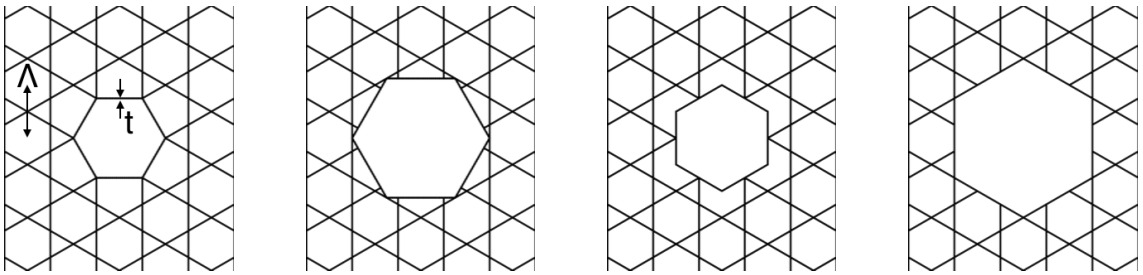

(a) (b) (c) (d)

Figure 2.1: The four cores used in this study. (a) single-cell defect offset 30° as compared to lattice hexagons. Indicated within are the pitch Λ and glass thickness t. (b) Larger core in the same orientation as (a). (c) Core in same orientation as lattice hexagons. (d) 7-cell defect in same orientation as (c).

For a material of a given thickness t and refractive index n, there can be found resonances where incident light of wavelength λ reflected from the material's two in-

terfaces destructively interfere. These wavelengths are given by $\lambda = \frac{2t\sqrt{n^2-1}}{m}$ where m is a natural number. All modeled geometries were set to a transverse glass thickness of $t = 0.0346\Lambda$, implying that the normalized resonance frequencies in our case are found at $\Lambda/\lambda = m(13.5954)$. Considering the glass surrounding the core of our fiber, we should expect to find no guided mode at these resonance frequencies.

2.1 Effects of geometric self-similarity

With infinitely thin boundaries the self-similarly of the kagome lattice would be exact, and we need not worry about glass resonance since it is inversely proportional to glass width. However, given the finite thickness of our glass walls we must take into account that the different scales will have different glass width to lattice pitch ratios. We therefore calculated explicitly the modes for the next level scale kagome lattice. In reference [28] the modes of the base lattice are rescaled in an attempt to predict dispersion of overlaid lattices and defects. We would like to point out that this is inaccurate since the major perturbation seen in the base lattice is near the glass resonance of the core surround and by rescaling the base lattice modes they have rescaled this resonance as well. The dispersion of modes found in a hexagonal air hole in the kagome lattice–even if this air hole is a defect–has been shown to be reasonably well predicted by the dispersion calculated for modes of a single dielectric tube [10,28]. The effective index of a dielectric tube is given by $n_{eff} = 1 - \frac{1}{2}\left(\frac{u_{mn}\Lambda}{2\pi R\alpha}\right)^2$, where α is normalized frequency, u_{mn} is the nth zero of the mth Bessel function J_m, and the radius R of the air hole is approximated by $R = \frac{1}{2}(R_1 + R_2)$ where R_1 is the apothem and R_2 is the circumradius of the hexagonal air hole. Since dielectric tube dispersion is in terms of cylindrical Bessel functions, we shall refer to these as 'cylinder modes' for the remainder of this work. For comparison, we plot below in Fig. 2.2 the modes found explicitly for the 3Λ case rescaled by the base lattice pitch along

with the corresponding cylinder modes, the base lattice modes rescaled to predict the 3Λ case, and the base lattice modes. We see that the rescaled lattice modes appear to be better predictors at frequencies below ∼4 and the cylinder modes are a better approximation at higher frequency. Since the low frequency edge is avoided in applications, we believe the cylinder modes are of more use. Also pictured in this figure are the defect modes for the geometry shown in Fig. 2.1d which is basically a hexagonal air-hole of the 3Λ scale lattice. Notice that the defect modes show excellent agreement with the 3Λ lattice modes and even the base lattice modes show some overlap with the higher order modes. This shows that a higher order circularly symmetric mode from one of the larger scale lattices can be expected to coincide with the fundamental or other low order circularly symmetric mode of the small scale lattice. We can furthermore expect the same thing in the case of a defect in the lattice. Essentially, modes in the hollow defect are possible because the lattice itself shows modes within its hollow regions. Following this logic, higher order circularly symmetric modes of the large scale sub-lattices such that the central spot fits within the defect should coincide with modes found in the defect as illustrated in Fig. 2.3.

The frequency of the equivalent modes of a large scale lattice as compared to those of the base lattice should be approximately equal when normalized by the lattice pitch for that scale, and therefore will be of lower frequency when normalized by the base lattice pitch. Thus, in the case of a lattice extending to infinity there should be an ever increasing density of modes as we approach zero frequency. In the finite structure enclosed within a fiber, the density of modes at the lower frequency end will be limited by the largest sub-structure which can still be considered to be a subset of a kagome lattice. In the interest of time we approximated the modes for the next several scale levels with those for dielectric tubes of appropriate size–up to 13Λ based on largest scale hexagon seen in fibers in the literature [22]. For each scale

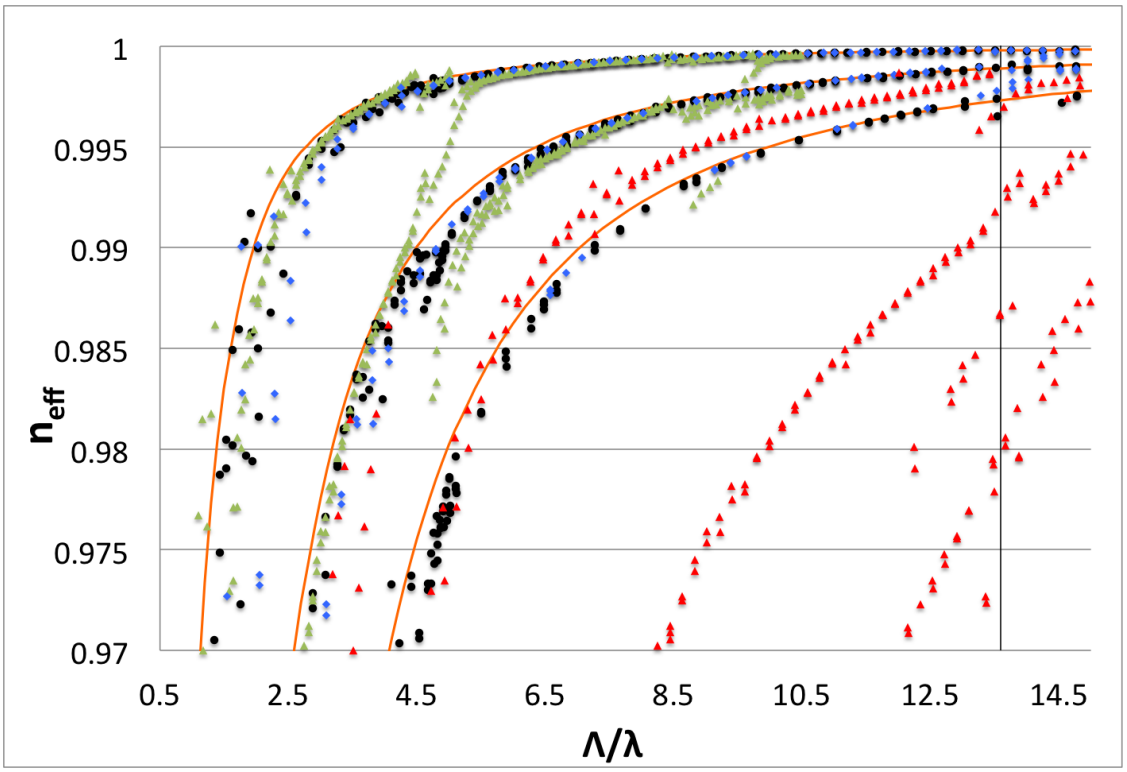

Figure 2.2: For comparison we plot the base lattice modes (red triangles), modes for 3Λ scale lattice (blue diamonds), rescaled base lattice modes (lime triangles), defect modes for the geometry shown in Fig. 2.1d (black circles), and cylinder modes for the defect (orange lines). Marked with the vertical line is the resonance of the core surround at $\Lambda/\lambda = 13.5954$.

$\Lambda' = m\Lambda$, m an odd number between 3 and 13, we calculated cylinder modes up to order $2m$ and these can be seen in Fig. 2.4. Interestingly, we observe some empty regions as well as regions with denser sets of these cylinder mode approximations. Focusing on the low frequency end, where the curves are all very steep, we see that this set of modes is responsible for the lack of defect modes found at low frequency since a laser with a nonzero linewidth launched into the core will try to couple to many modes of different spatial profiles and effective indices.

Next we overlapped the defect modes for each geometry and the cylinder modes for each scale, removing any cylinder modes which did not overlap the defect modes.

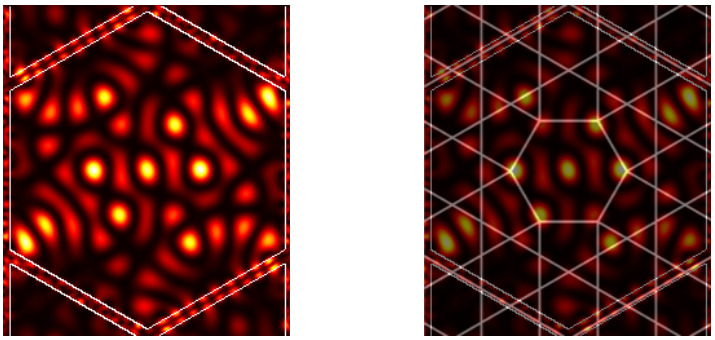

(a) (b)

Figure 2.3: (a) A higher order mode with circularly symmetric center. (b) Kagome lattice with a defect shown superposed over the mode shown in (a).

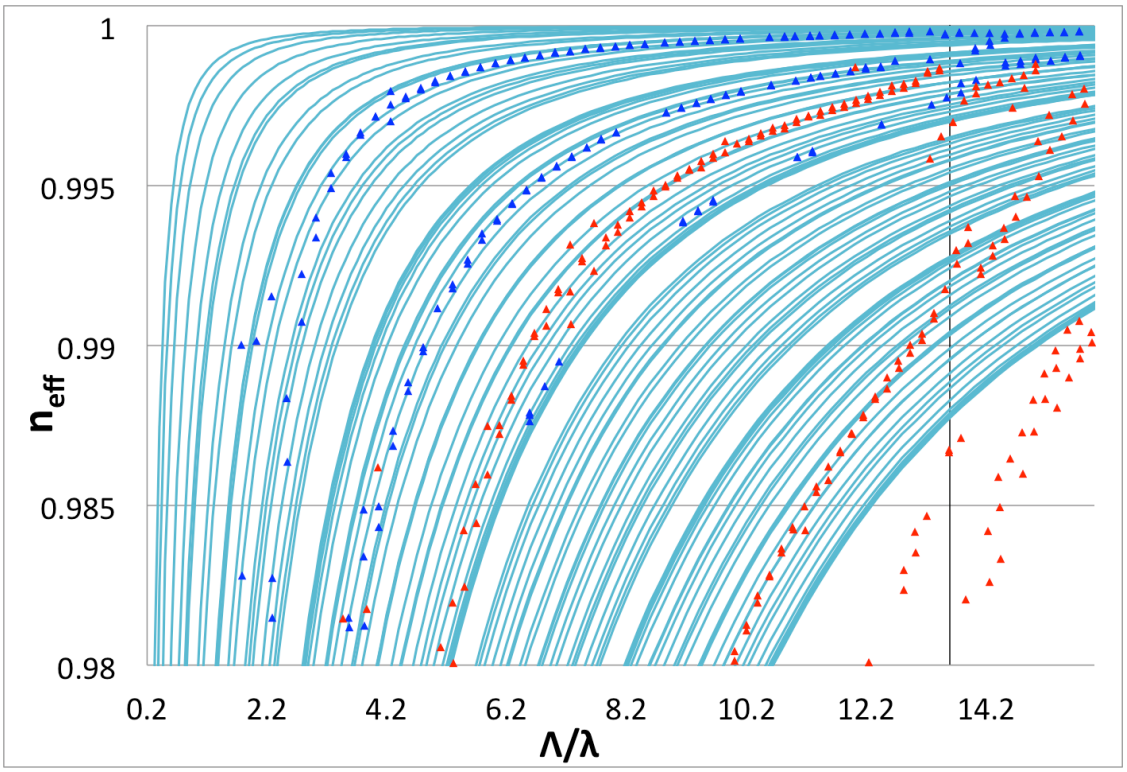

Figure 2.4: Base lattice modes shown in red triangles, modes for 3Λ scale lattice shown in blue triangles, and modes for other relevant scales shown with teal lines. Marked with the vertical line is the resonance of the core surround at $\Lambda/\lambda = 13.5954$.

This is illustrated below in Figs 2.5 – 2.8 going from smallest to largest core. The defect modes are seen to be enveloped by a set of cylinder modes where some are a better approximation at lower frequency and others are a better approximation at higher frequency. Additionally, for each core the defect modes are seen to overlap more cylinder modes and become scattered at the low frequency end. These observations support the idea that the defect modes stem from the lattice and that the diverging cylinder mode curves at the low end lead to no guided mode in experiment. An experimental study might be able to explore wether a defect mode found overlapping a dense sets is less lossy than one found in an empty region.

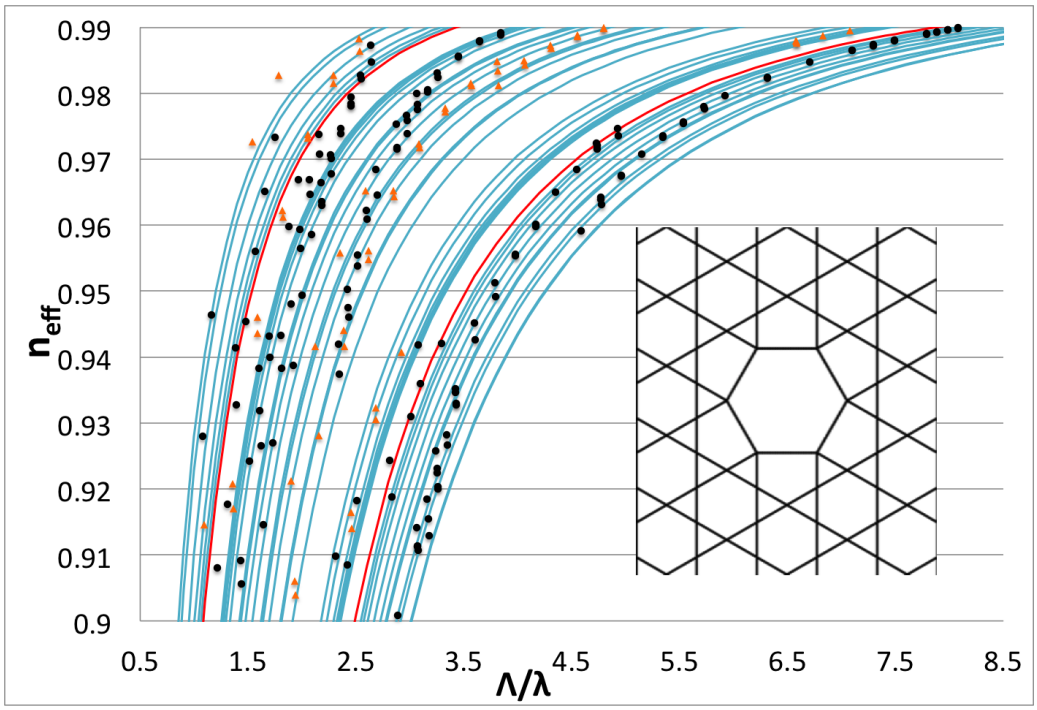

(a)

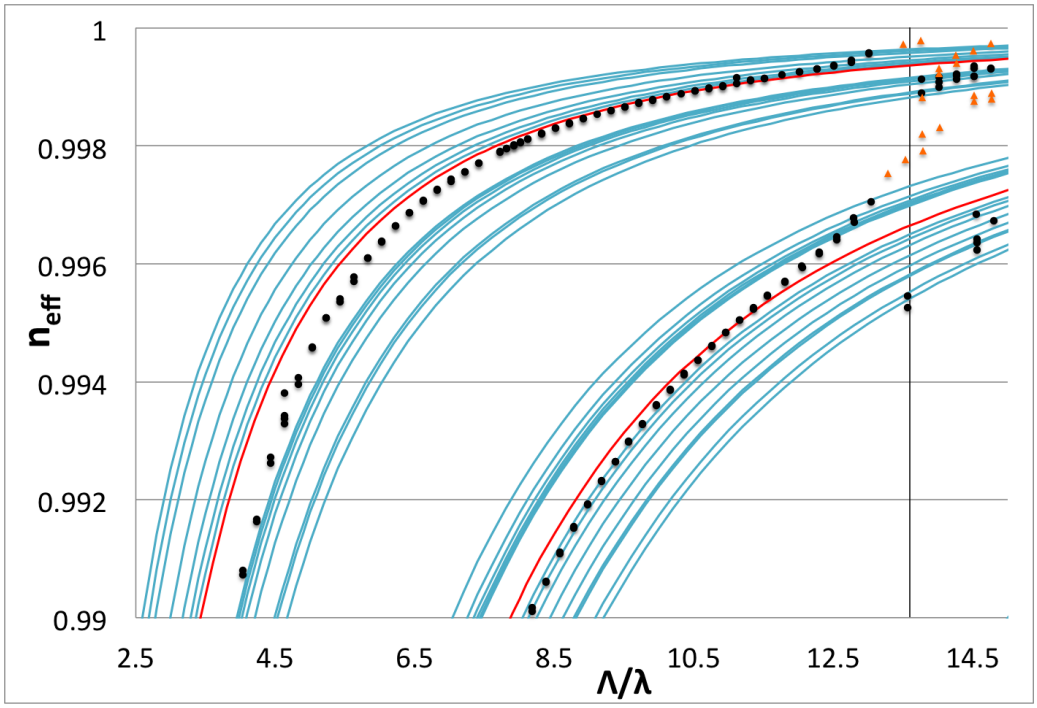

(b)

Figure 2.5: Defect mode dispersion (black circles) for the geometry shown in the inset of (a) along with dispersion for nearby cylinder modes (teal lines), cylinder modes for the defect mode size (red lines), and nearby modes from the 3Λ scale lattice (orange triangles). (a) shows the lower frequency envelope and (b) shows the higher frequency envelope.

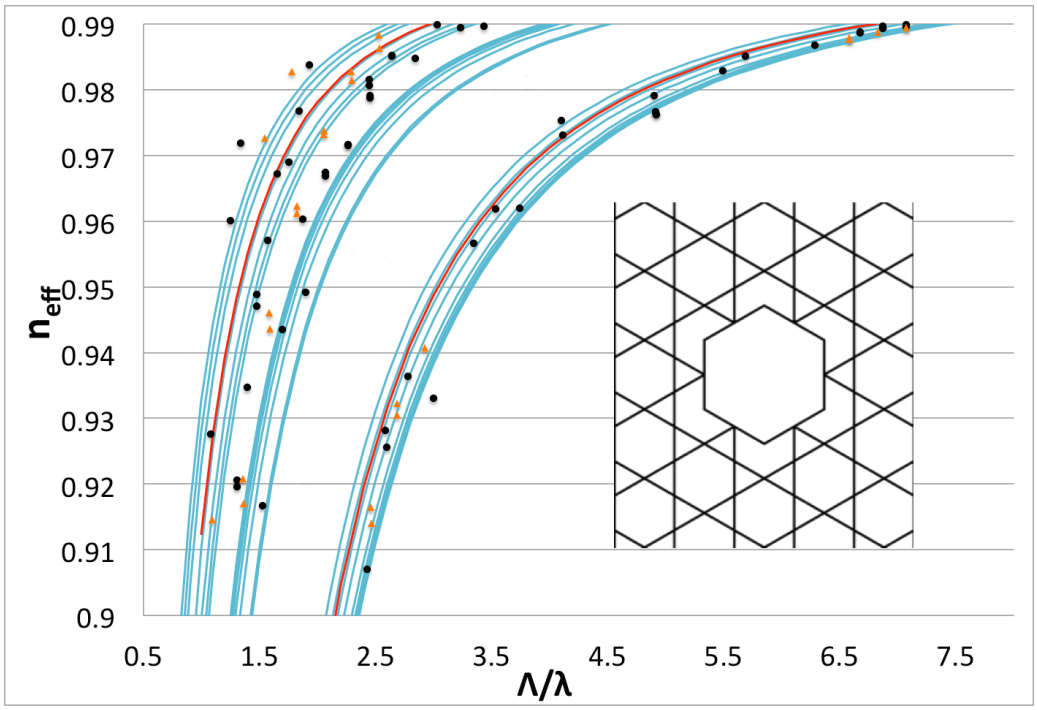

(a)

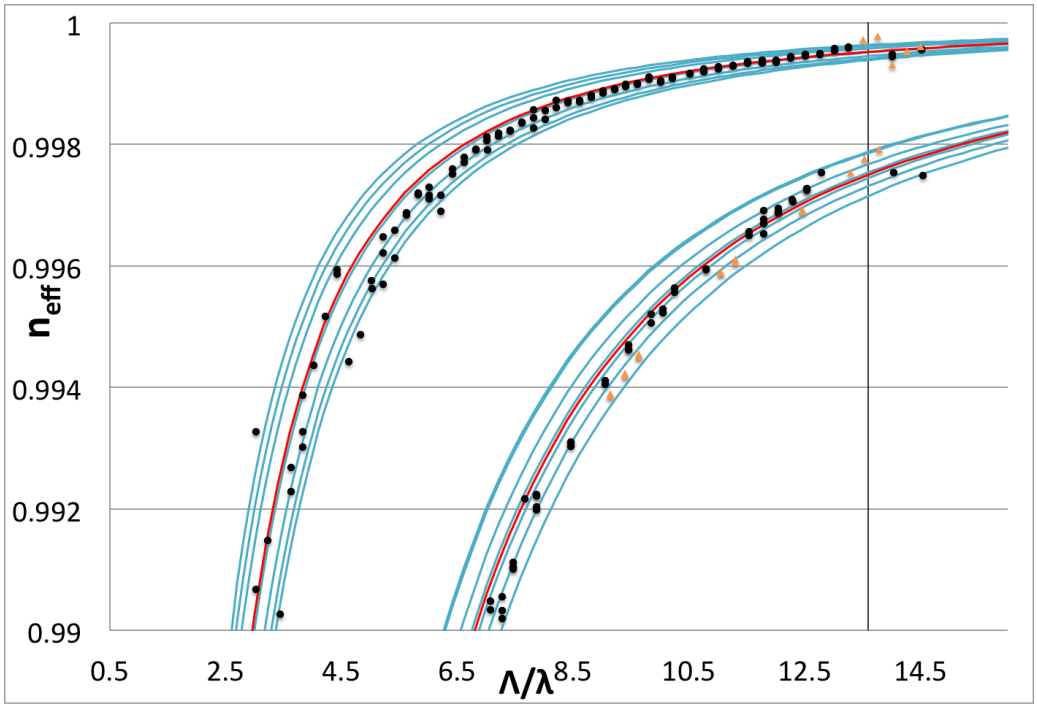

(b)

Figure 2.6: Defect mode dispersion (black circles) for the geometry shown in the inset of (a) along with dispersion for nearby cylinder modes (teal lines), cylinder modes for the defect mode size (red lines), and nearby modes from the 3Λ scale lattice (orange triangles). (a) shows the lower frequency envelope and (b) shows the higher frequency envelope.

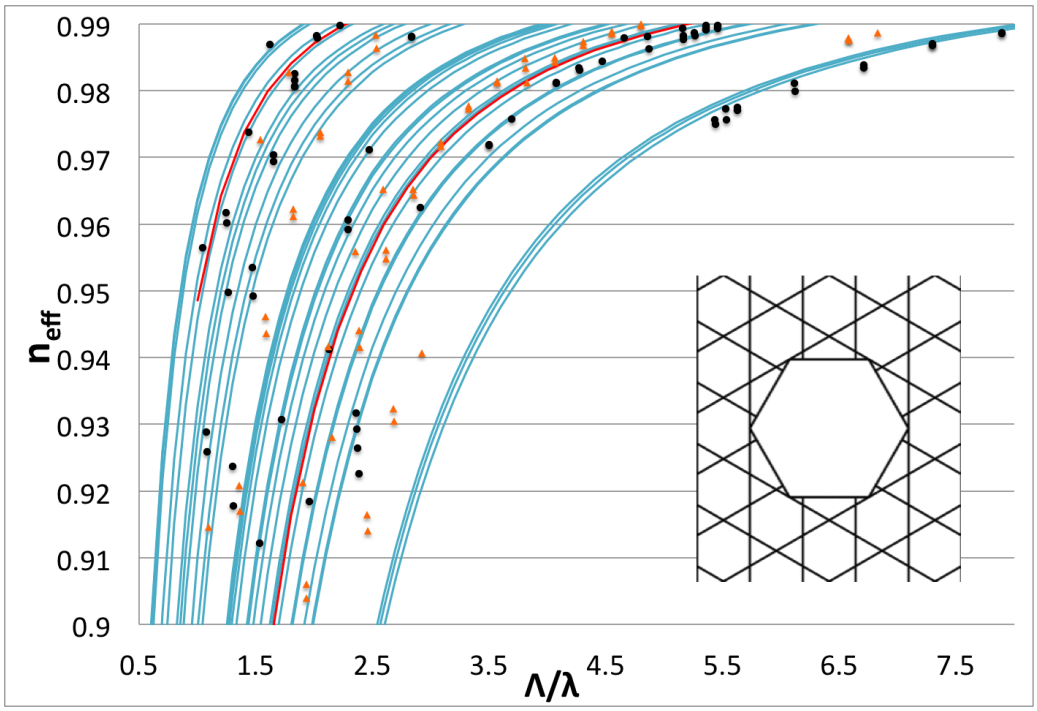

(a)

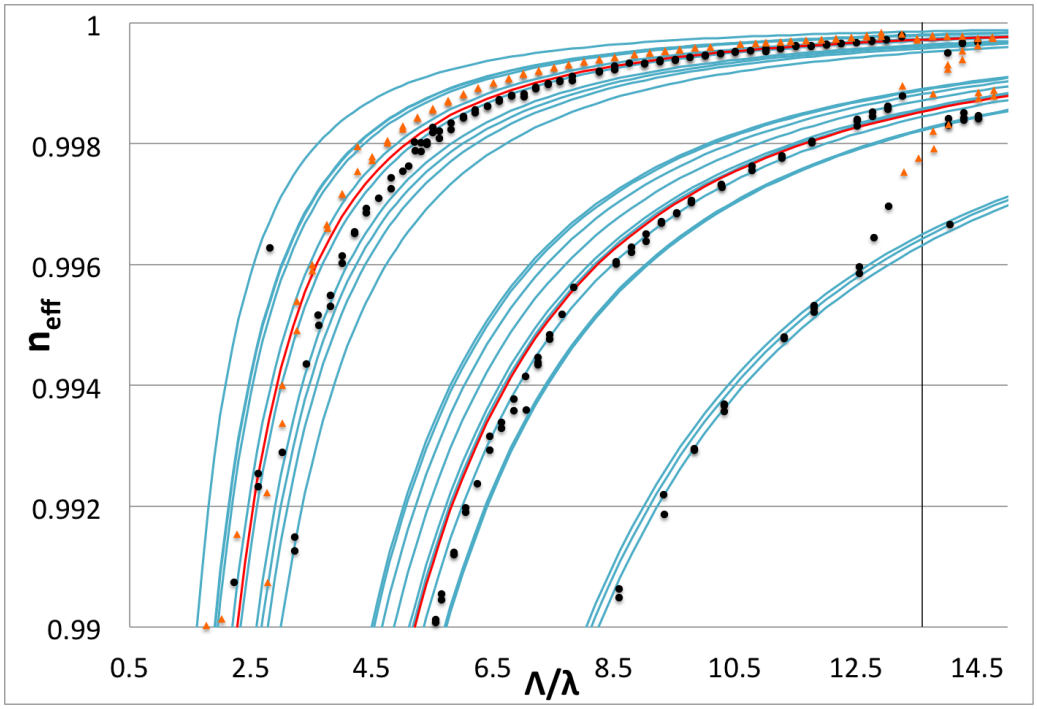

(b)

Figure 2.7: Defect mode dispersion (black circles) for the geometry shown in the inset of (a) along with dispersion for nearby cylinder modes (teal lines), cylinder modes for the defect mode size (red lines), and nearby modes from the 3Λ scale lattice (orange triangles). (a) shows the lower frequency envelope and (b) shows the higher frequency envelope.

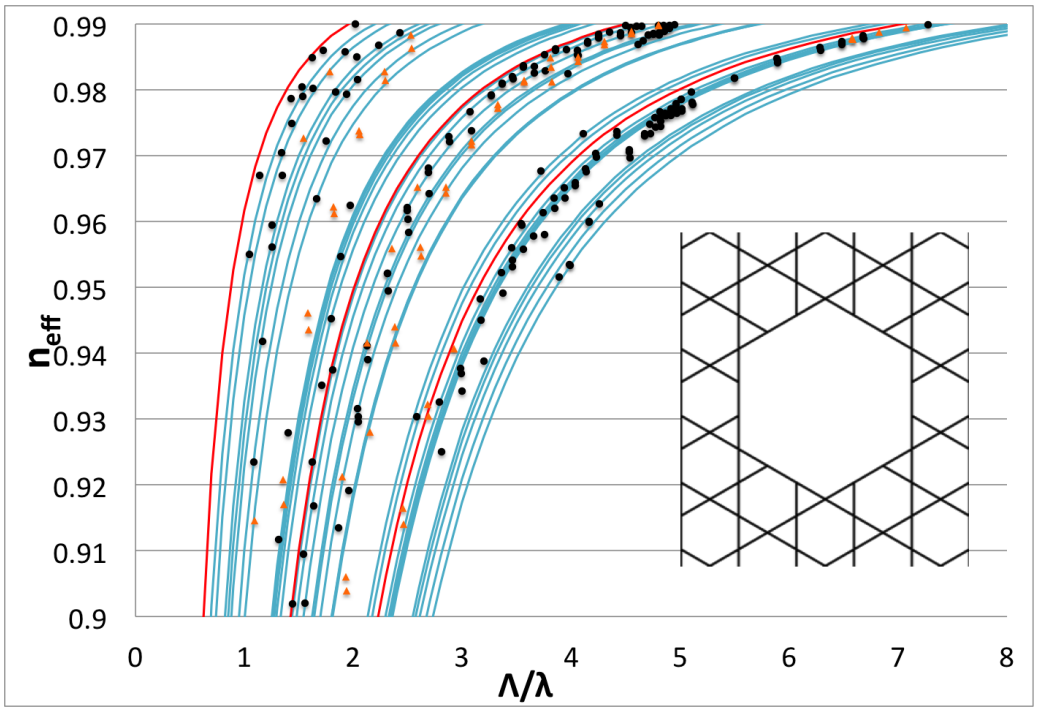

(a)

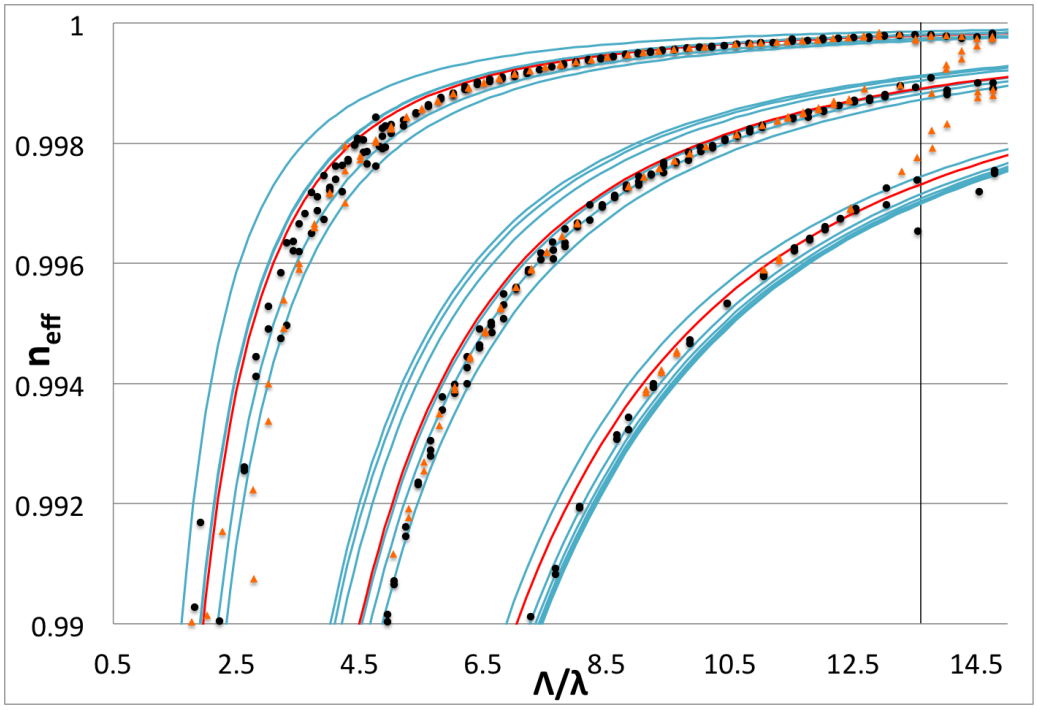

(b)

Figure 2.8: Defect mode dispersion (black circles) for the geometry shown in the inset of (a) along with dispersion for nearby cylinder modes (teal lines), cylinder modes for the defect mode size (red lines), and nearby modes from the 3Λ scale lattice (orange triangles). (a) shows the lower frequency envelope and (b) shows the higher frequency envelope.

2.2 Band-gap related sub-structures

To explore the effects of band-gaps on guidance in the kagome lattice we constructed several models. Beginning with the concentric hexagon model of the kagome lattice we found the band-gaps for a Bragg mirror with matching parameters. For this particular multilayer film we found the existence of three narrow band-gaps centered around low normalized frequencies of 0.57, 1.11, and 1.61. PBGs are always present for a multilayer film, however, complete band-gaps are only present for light incident normal to the stack [29]. Therefore, we don't expect these to play any significant role in guidance.

In the literature can be found 2D band-gap structures in the form of tubes arranged in either a triangular lattice or a honeycomb lattice [30]. In Fig. 2.9 we highlight a hexagonal and triangular subsection of the kagome lattice to be broken off at the vertices in order to be viewed as either a triangular lattice of hexagonal tubes or as a honeycomb lattice of triangular tubes. We began by looking for band-gaps in the triangular lattice of hexagonal tubes and found that at the non-zero starting distance we chose, the arrangement did display band-gaps and these dipped below the air-line minutely. However, as we decreased the distance between tubes we observed the band-gaps rise above the air-line and then disappear altogether. Therefore, we concluded this model to not be useful for guidance in a kagome lattice. With that result we abandoned the search for band-gaps in the honeycomb lattice as we expected a similar outcome.

To explore the effect of any band-gaps stemming from the node sites of the kagome lattice, we defined an effective node radius as half the average width of the glass when crossed along the axis connecting the two hexagons on either side of the node and an axis perpendicular to this. $r_{node} = \frac{t}{2}(\frac{1}{\sqrt{3}} + 1)$, where t is the transverse thickness of

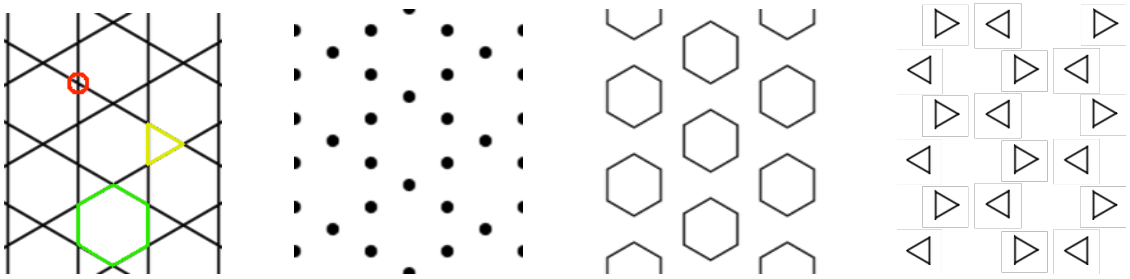

(a) (b) (c) (d)

Figure 2.9: (a) The different subset units of the kagome lattice highlighted. (b) The nodes circled in red remain fixed at their location in the base lattice, while the hexagons (green) and triangles (yellow) would be broken at the vertices and separated spatially to be a (c) triangular and (d) honeycomb 'tube' lattice, respectively.

the glass struts. The lattice air-hole modes were found to definitely be influenced by the band-gaps found from the kagome-node lattice as can be seen below in Fig. 2.10. No air-hole modes for the kagome lattice were found to exist within the band-gap and even the continuity of the dispersion is seen to be cut by a band-gap dipping below the air-line, suggesting that the band-gaps stemming from the nodes play a role in defect guidance. Additionally, this band-gap coincides with a low DOS region for the full lattice. Also shown in Fig. 2.10 are the air-hole modes for the 3Λ scale kagome lattice and the band-gaps for the equivalent nodes. The relative node size for this scale is smaller compared to the base lattice, and once again we see the kagome lattice air-hole modes are bounded above by the band-gap. However, the gap dips only minutely below the air-line, and thus, we expect larger nodes to be beneficial for guidance.

Next we mapped dispersion for modes in a node lattice and a node lattice with a '7-cell' defect in order to compare these to the analogous cases with a full kagome lattice. In Fig. 2.11 we show that modes similar in profile to those found in the full kagome lattice were found in the node lattice, but dispersion for these two sets

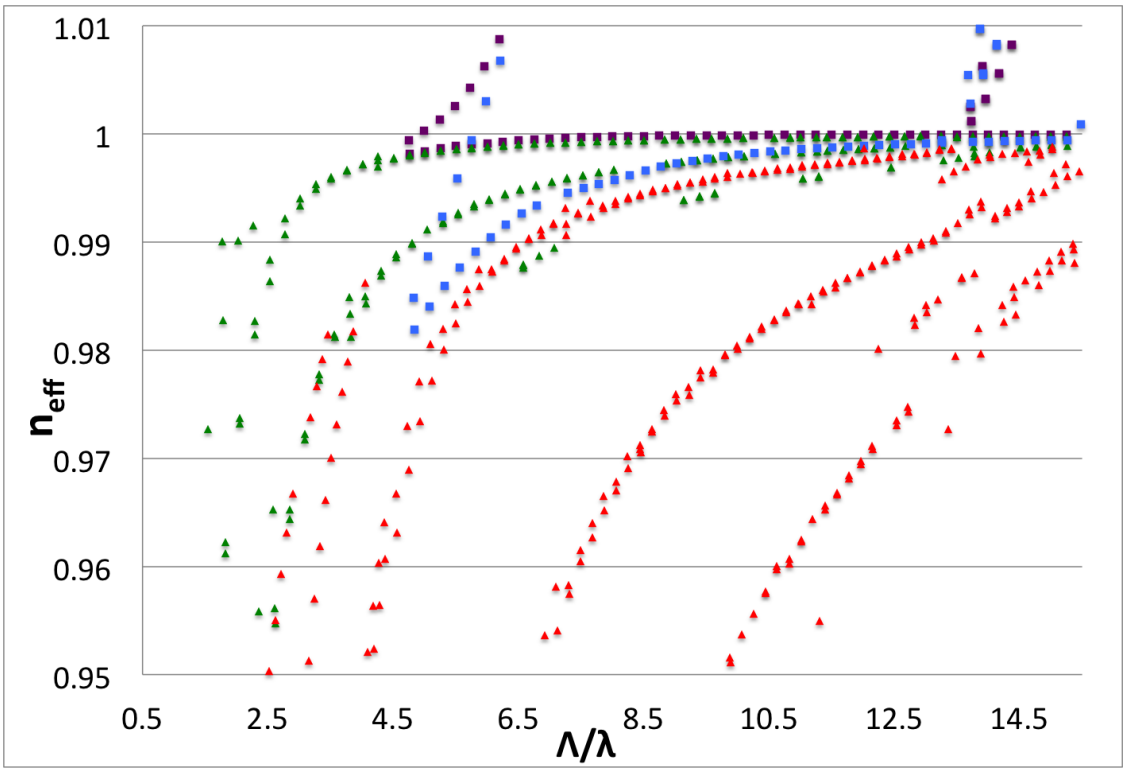

Figure 2.10: Base lattice modes shown in red triangles, band-gaps for matching node size shown in blue squares. 3Λ scale lattice modes shown in green triangles, and band-gaps for matching nodes for 3Λ scale node size shown in purple squares. Note how the band-gap stemming from the base lattice node size cuts into the dispersion curve for the base lattice modes, unlike for the 3Λ scale.

overlapped only slightly. For the 7-cell defect, however, Fig. 2.12 shows that the mode profile as well as the dispersion of defect modes in each case is seen to agree very well especially as frequency is increased, suggesting that the nodes of the kagome lattice are a major contributor to defect guidance.

Defect mode dispersion going from smallest to largest core geometry can be seen in Figs. 2.13 – 2.16 along with the band-gaps from the node lattices corresponding to the base lattice and 3Λ lattice and the modes for those two lattices to see where they fall in relation to each other. Comparing these figures, we see that the effect on dispersion from enlarging the core is to push the low frequency edge to lower

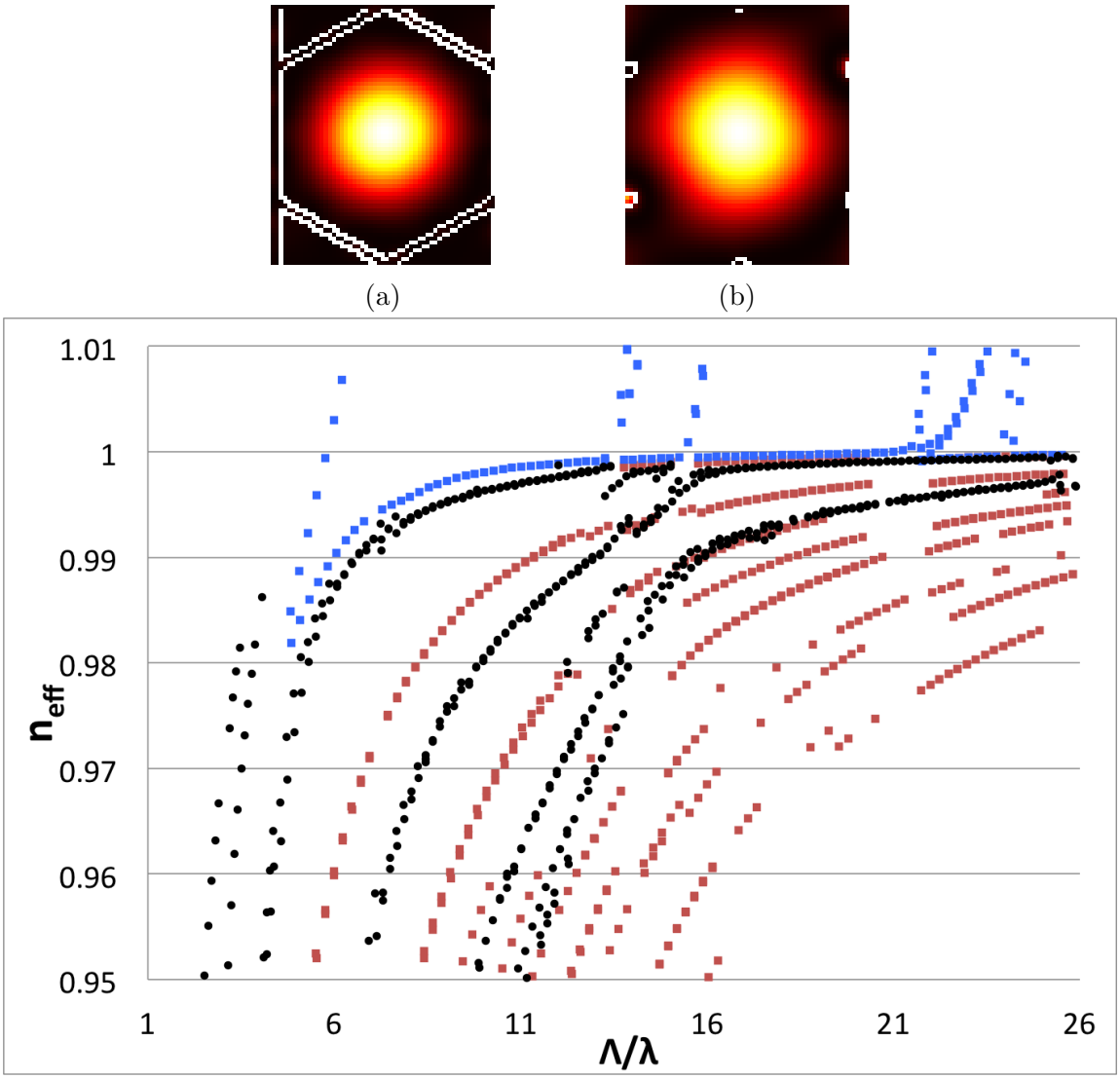

(a) (b)

(c)

Figure 2.11: (a) Mode found in kagome lattice. (b) Mode found in node lattice. (c) Comparison of full lattice modes (black) to analogous modes found in node lattice (red), and band-gaps from the node lattice (blue).

frequency while also flattening the curve and lifting it closer to the air line for higher frequencies. Near the glass resonance we observe that the perturbation from this resonance is greatly reduced for the 7-cell defect. This can be explained by the fact that the defect modes are further away in effective index compared to the base lattice

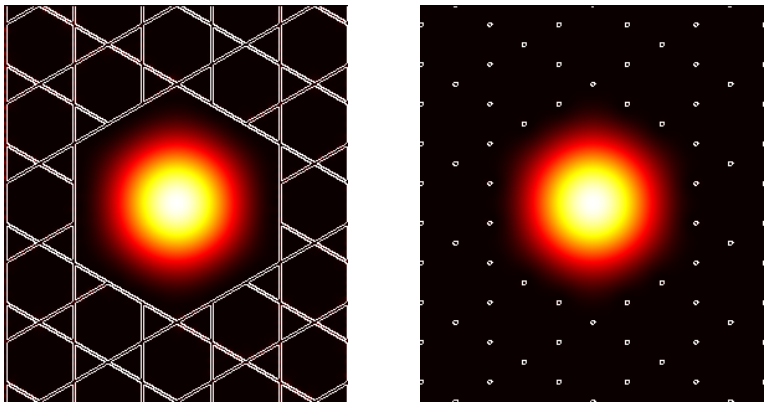

(a) (b)

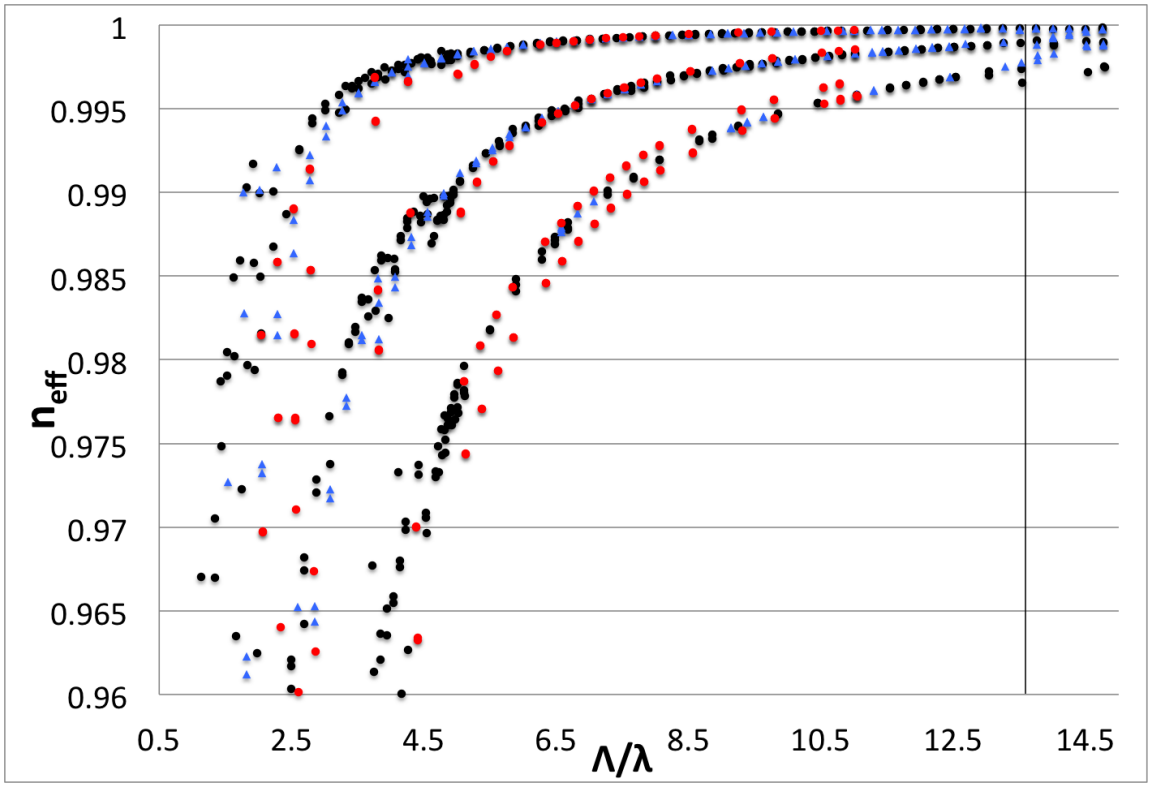

(c)

Figure 2.12: (a) 7-cell defect mode found in kagome lattice. (b) '7-cell' defect mode found in node lattice at about the same frequency. (c) Comparison of defect modes found in full kagome lattice (black) to analogous defect modes found in node lattice (red).

modes as well as further encompassed within the band-gaps of the base lattice nodes. The small perturbation seen in Fig. 2.16 also indicates that perhaps the destructive effects of the glass resonance can be overcome.

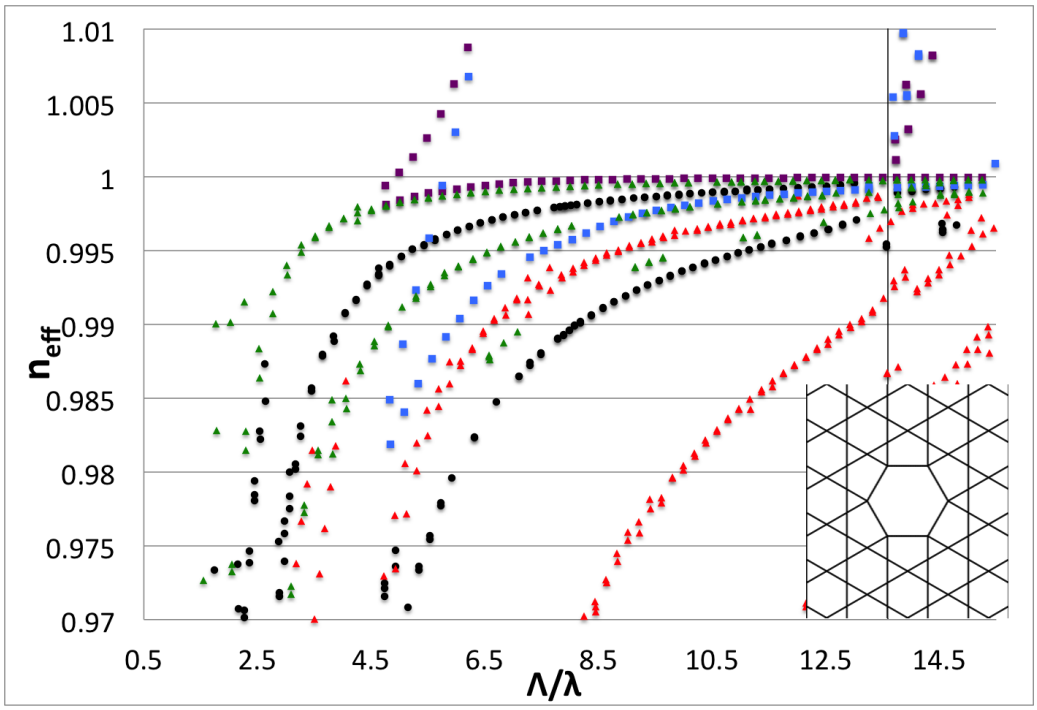

(a)

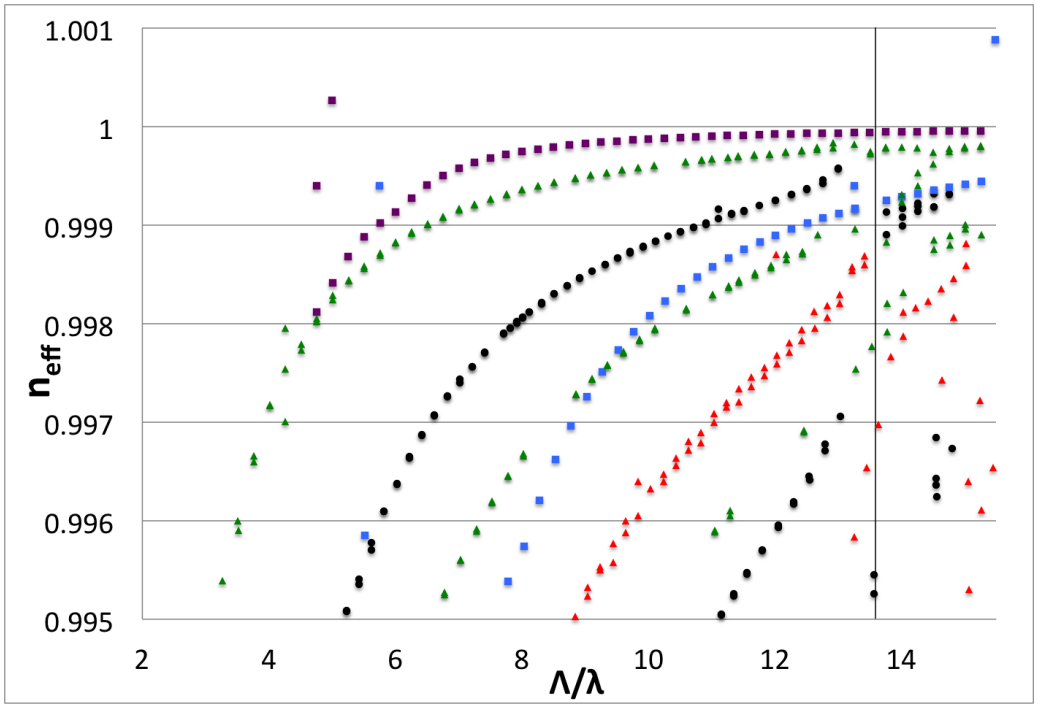

(b)

Figure 2.13: Dispersion map of low order circularly symmetric modes (black circles) for core geometry shown in inset of (a), along with base lattice modes (red triangles), band-gaps for the base lattice node size (blue squares), 3Λ scale lattice modes (green triangles), and band-gaps for the 3Λ scale node size (purple squares). (b) is a zoomed in version of (a).

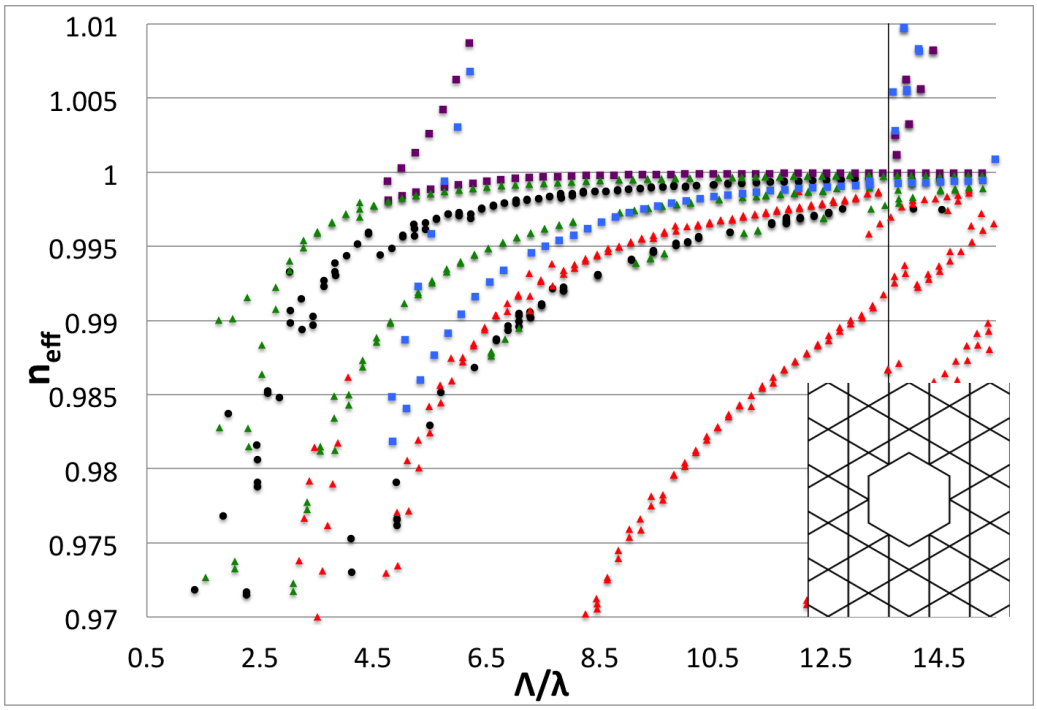

(a)

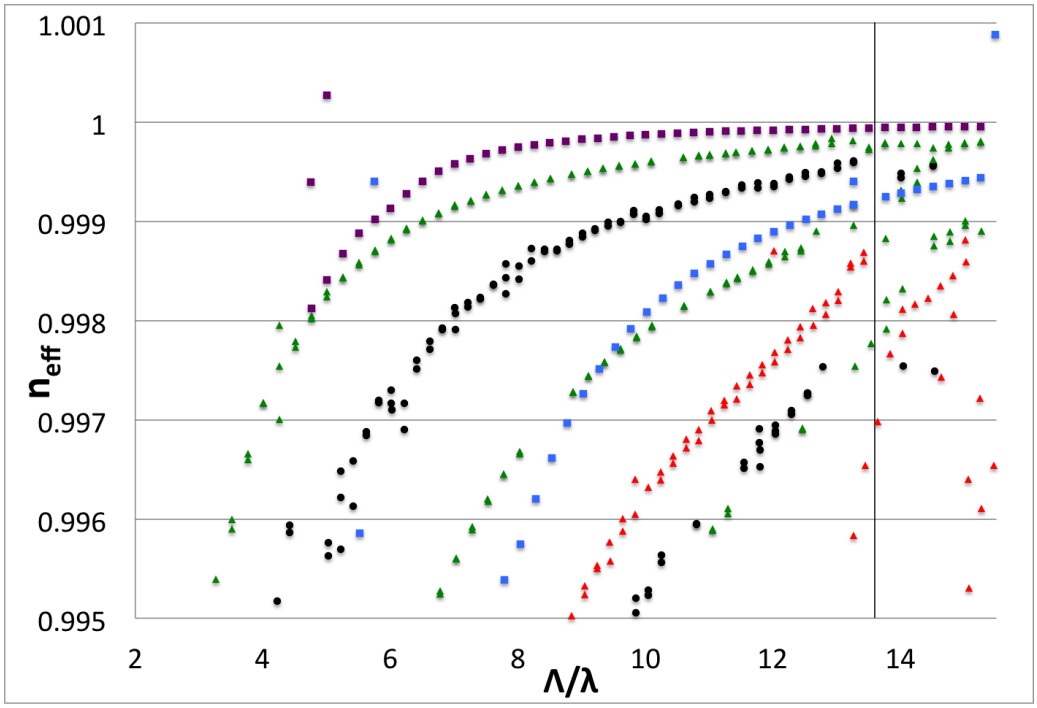

(b)

Figure 2.14: Dispersion map of low order circularly symmetric modes (black circles) for core geometry shown in inset of (a), along with base lattice modes (red triangles), band-gaps for the base lattice node size (blue squares), 3Λ scale lattice modes (green triangles), and band-gaps for the 3Λ scale node size (purple squares). (b) is a zoomed in version of (a).

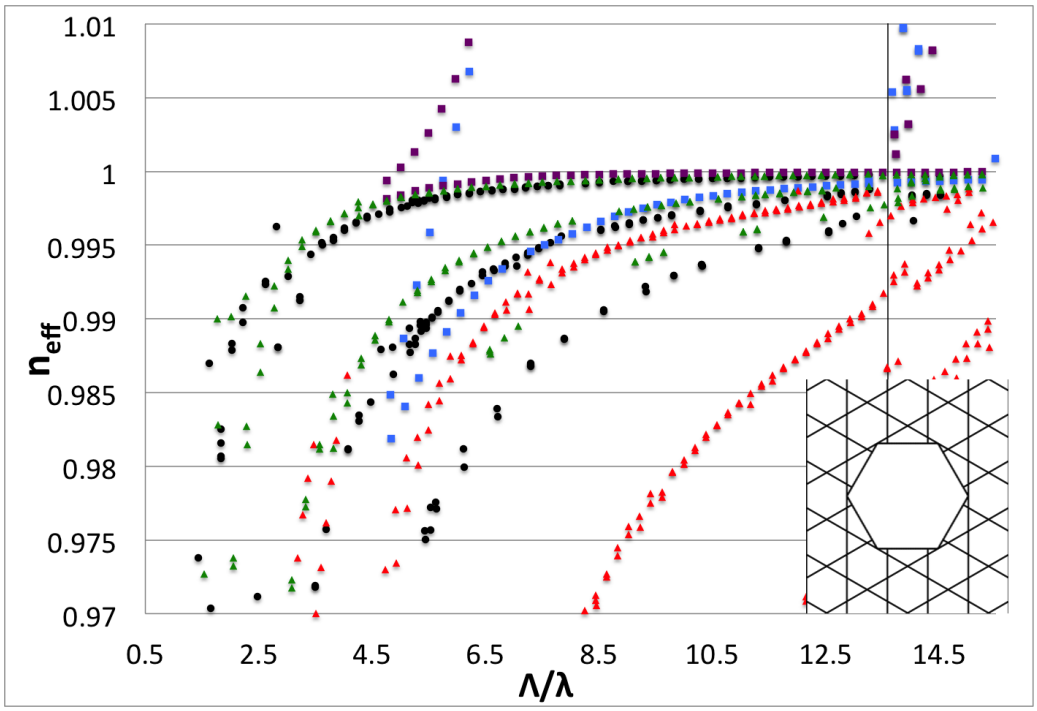

(a)

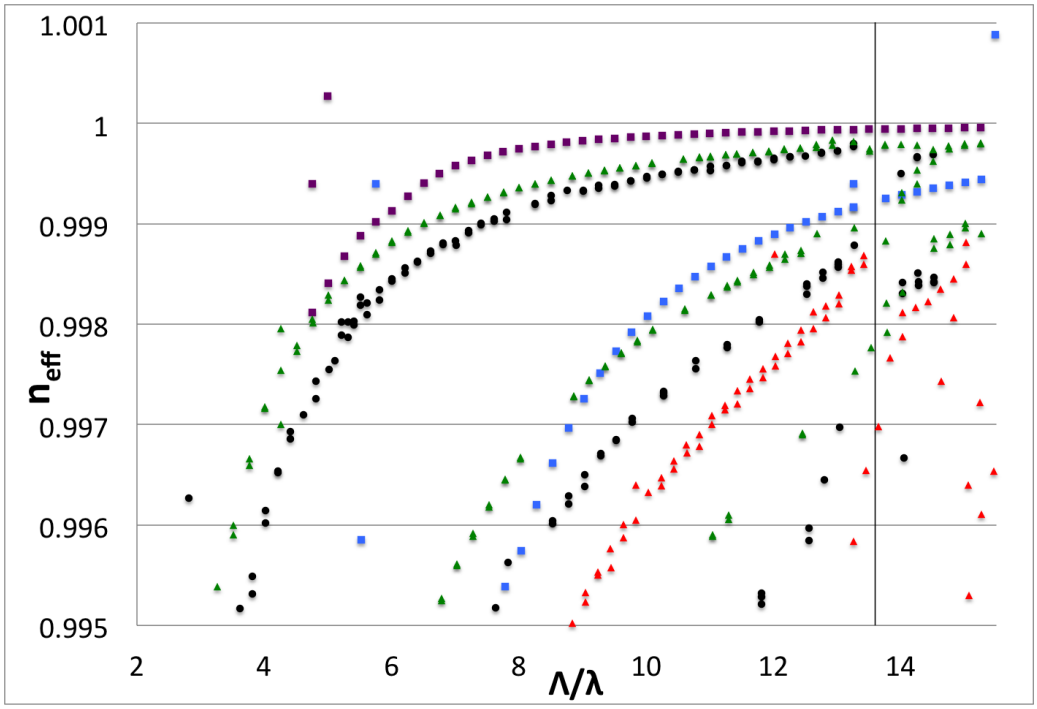

(b)

Figure 2.15: Dispersion map of low order circularly symmetric modes (black circles) for core geometry shown in inset of (a), along with base lattice modes (red triangles), band-gaps for the base lattice node size (blue squares), 3Λ scale lattice modes (green triangles), and band-gaps for the 3Λ scale node size (purple squares). (b) is a zoomed in version of (a).

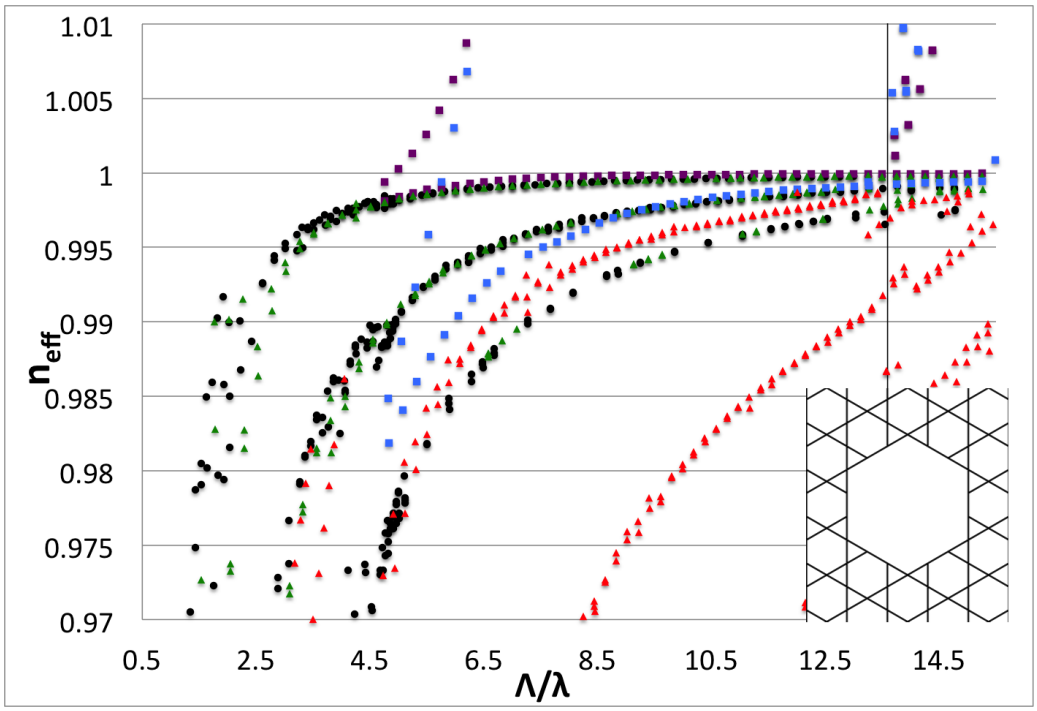

(a)

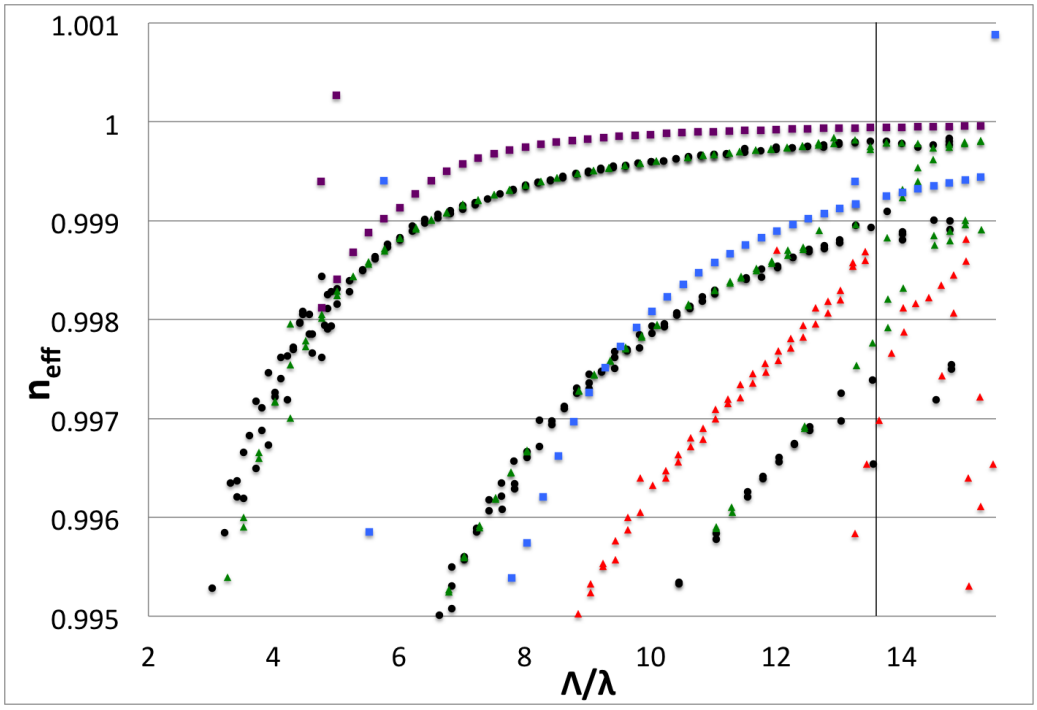

(b)

Figure 2.16: Dispersion map of low order circularly symmetric modes (black circles) for core geometry shown in inset of (a), along with base lattice modes (red triangles), band-gaps for the base lattice node size (blue squares), 3Λ scale lattice modes (green triangles), and band-gaps for the 3Λ scale node size (purple squares). (b) is a zoomed in version of (a).

3. OUTLOOK AND CONCLUSIONS

We conclude with some design and operating suggestions which we believe will enhance guidance in kagome clad fibers. First, we note that the low frequency region remains to be avoided. In this region the cylinder mode curves are all very steep and correspond to low order circularly symmetric modes of large scale lattices. Since any real laser has a nonzero line width this implies that the light will try to couple to a number of modes not only with very different propagation constants but also very different mode profiles where some of those mode profiles may be larger than the defect size, essentially killing the mode. Strut thickness, especially surrounding the core, appears to be the major perturbing factor dictating high loss regions through glass resonance effects. The location of this resonance is inversely proportional to the thickness of the glass, and therefore thinning the struts should consequently widen the regions of guidance. Increasing the node size should enlarge the region a band-gap covers below the air-line while also increasing the number of gaps dipping below the air-line. This will serve to separate the indices of refraction of the core and lattice modes while also enclosing the core mode further within the band-gap. Equivalently, and of more use given the suggestion for thin struts, increasing the refractive index at the node sites should have the same effect. To accomplish this we suggest modifying the glass tubes, perhaps through chemical vapor deposition, before stacking them into a preform for drawing, as in Fig. 3.1.

Contrary to the current literature we expect to see an improvement in guidance with an increase in number of cladding rings, however, because of the way the kagome lattice scales we expect that very many cladding rings are required to see a significant improvement. For a given set of lattice parameters, designing the core so that it's

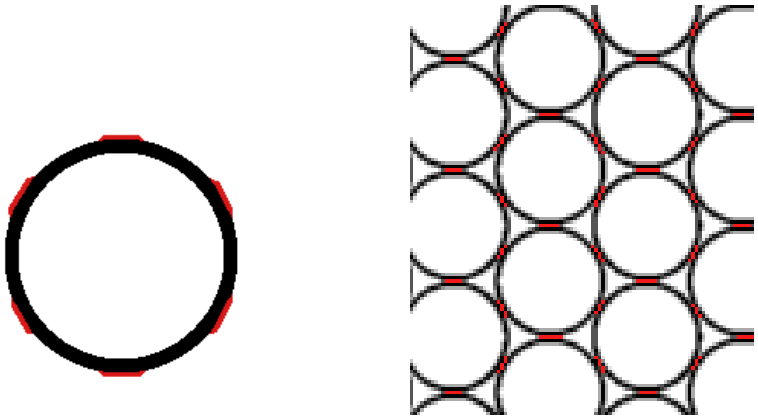

(a) (b)

Figure 3.1: (a) A modified glass tube, where the modified segments are indicated in red. (b) A preform stack of glass tubes of the type shown in (a), arranged so that the modified segments of the tube lie at the node sites.

expected dispersion lies along a dense set of large-scale-lattice modes may also aid in reducing loss.

We have one final remark regarding the coherence of the fundamental mode. Between the high loss regions bounded below by the low frequency edge and above by the first glass resonance, the core modes show some perturbations but not enough perturbation that we expect modes to become mixed. This supports the idea that the mode is coherent between these boundaries, and we expect also between subsequent glass resonances. With the design considerations mentioned above we believe it may be possible for the constructive interference which makes guidance in this structure possible to beat out the destructive interference from the core surround, bridging the gap between these low loss regions and making possible a fiber with ultra wide regions of guidance.

REFERENCES

[1] G J Pearce, G S Wiederhecker, C G Poulton, S Burger, and P J Russell. Models for guidance in kagome-structured hollow-core photonic crystal fibres. *Opt. Exp.*, 15:12680–12685, 2007.

[2] S Fevrier, B Beaudou, and P Viale. Understanding origin of loss in large pitch hollow-core photonic crystal fibers and their design simplification. *Opt. Exp.*, 18:5142–5150, 2010.

[3] M Alharbi, T Bradley, B Debord, C Fourcade-Dutin, D Ghosh, L Vincetti, F Gérôme, and F Benabid. Hypocycloid-shaped hollow-core photonic crystal fiber part ii: Cladding effect on confinement and bend loss. *Optics Express*, 21:28609–28616, 2013.

[4] F Benabid, P J Roberts, F Couny, and P S Light. Light and gas confinement in hollow-core photonic crystal fibre based photonic microcells. *Journal of the European Optical Society*, 4:09004, 2009.

[5] Y Y Wang, F Couny, P S Light, B J Mangan, and F Benabid. Compact and portable multiline uv and visible raman lasers in hydrogen-filled hc-pcf. *Optics Letters*, 35:1127–1129, 2010.

[6] F Emaury, C Fourcade-Dutin, C Saraceno, M Trant, O Heckl, Y Y Wang, C Schriber, F Gérôme, T Südmeyer, F Benabid, and U Keller. Beam delivery and pulse compression to sub-50 fs of a modelocked thin-disk laser in a gas-filled kagome-type hc-pcf fiber. *Optics Express*, 21:4986–4994, 2013.

[7] F Couny, F Benabid, P J Roberts, P S Light, and M G Raymer. Generation and photonic guidance of multi-octave optical-frequency combs. *Science*, 318:1118–

1121, 2007.

[8] T Balciunas, C Fourcade-Dutin, G Fan, T Witting, A A Voronin, A M Zheltikov, F Gerome, G G Paulus, A Baltuska, and F Benabid. A strong-field driver in the single-cycle regime based on self-compression in a kagome fibre. *Nature Communications*, 6:6117, 2015.

[9] A M Zheltikov. Colors of thin films, anti resonant phenomena in optical systems, and the limiting loss of modes in hollow optical waveguides. *Physics-Uspekhi*, 51:591–600, 2008.

[10] L Vincetti and V Setti. Waveguiding mechanism in tube lattice fibers. *Opt. Exp.*, 18:23133–23146, 2010.

[11] Y Y Wang, N V Wheeler, F Couny, P J Roberts, and F Benabid. Low loss broadband transmission in hypocycloid-core kagome hollow-core photonic crystal fiber. *Opt. Lett.*, 36:669–671, 2011.

[12] B Debord, M Alharbi, T Bradley, C Fourcade-Dutin, Y Y Wang, L Vincetti, F Gérôme, and F Benabid. Hypocycloid-shaped hollow-core photonic crystal fiber part i: Arc curvature effect on confinement loss. *Optics Express*, 21:28597–28608, 2013.

[13] B Debord, M Alharbi, A Benoît, D Ghosh, M Dontabactouny, L Vincetti, J.-M. Blondy, F Gérôme, and F Benabid. Ultra low-loss hypocycloid-core kagome hollow-core photonic crystal fiber for green spectral-range applications. *Optics Letters*, 39:6245–6248, 2014.

[14] F H Stillinger and D R Herrick. Bound states in the continuum. *Physical Review A*, 11:446–454, 1975.

[15] A M Zheltikov. Microstructure-fiber frequency converters. *Laser Phys. Lett.*, 1:220–233, 2004.

[16] R F Cregan, B J Mangan, J C Knight, T A Birks, P J Russell, P J Roberts, and D A Allan. Single-mode photonic band gap guidance of light in air. *Science*, 285:1537, 1999.

[17] C M Smith, N Venkataraman, M T Gallagher, D Müller, J A West, N F Borrelli, D C Allan, and K W Koch. Low-loss hollow-core silica/air photonic bandgap fibre. *Nature*, 424:657, 2003.

[18] S O Konorov, L A Mel'nikov, A A Ivanov, M V Alfimov, A V Shcherbakov, and A M Zheltikov. Diamond-shaped-core hollow photonic-crystal fiber. *Laser Phys. Lett.*, 2:366, 2005.

[19] F Benabid, J C Knight, G Antonopoulos, and P S Russell. Stimulated raman scattering in hydrogen-filled hollow-core photonic crystal fiber. *Science*, 298:399–402, 2002.

[20] P S Russell, P Hölzer, W Chang, A Abdolvand, and J C Travers. Hollow-core photonic crystal fibers for gas-based nonlinear optics. *Nature Photonics*, 8:278–286, 2014.

[21] S O Konorov, A M Zheltikov, P Zhou, A P Tarasevitch, and D von der Linde. Self-channeling of subgigawatt femtosecond laser pulses in a ground-state waveguide induced in the hollow core of a photonic crystal fiber. *Optics Letters*, 29:1521–1523, 2004.

[22] F Couny, F Benabid, and P S Light. Large-pitch kagome-structured hollow-core photonic crystal fiber. *Opt. Lett.*, 31:3574–3576, 2006.

[23] Y Y Wang, P S Light, and F Benabid. Core-surround shaping of hollow-core photonic crystal fiber via hf etching. *IEEE Photonics Tech. Lett.*, 20:1018–1020, 2008.

[24] A M Zheltikov. Isolated waveguide modes of high-intensity light fields. *Physics-Uspekhi*, 47:1205–1220, 2004.

[25] S G Johnson and J D Joannopoulos. Block-iterative frequency-domain methods for maxwell's equations in a planewave basis. *Optics Express*, 8:173–190, 2001.

[26] J B Nielsen, T Sondergaard, S E Barkou, A Bjarklev, J Broeng, and M B Nielsen. Two-dimensional kagome structure fundamental hexagonal photonic crystal configuration. *Electronics Letters*, 35:1736–1737, 1999.

[27] R Kitamura, L Pilon, and M Jonasz. Optical constants of silica glass from extreme ultraviolet to far infrared at near room temperature. *Applied Optics*, 46:8118–8133, 2007.

[28] H Perez, S Blakley, and A M Zheltikov. Modal analysis of kagome-lattice structures. *Laser Physics Letters*, 12:055102, 2015.

[29] J D Joannopoulus, S G Johnson, J N Winn, and R D Meade. *Photonic Crystals: Molding the Flow of Light*. Princeton University Press, 2008.

[30] A Bjarklev, J Broeng, and A S Bjarklev. *Photonic Crystal Fibres*. Springer US, 2003.